Structure-Based Mechanism for Oxidative Decarboxylation Reactions Mediated by Amino Acids and Heme Propionates in Coproheme Decarboxylase (HemQ)

Arianna I. Celis,[†] George H. Gauss,[†] Bennett R. Streit,[†] Krista Shisler,[†] Garrett C. Moraski,[†] Kenton R. Rodgers,[‡] Gudrun S. Lukat-Rodgers,[‡] John W. Peters,[†] and Jennifer L. DuBois*[,†]

[†]Department of Chemistry and Biochemistry, Montana State University, Bozeman, Montana 59717-3400, United States
[‡]Department of Chemistry and Biochemistry, North Dakota State University, Fargo, North Dakota 58108-6050, United States

S *Supporting Information*

ABSTRACT: Coproheme decarboxylase catalyzes two sequential oxidative decarboxylations with H_2O_2 as the oxidant, coproheme III as substrate and cofactor, and heme *b* as the product. Each reaction breaks a C—C bond and results in net loss of hydride, via steps that are not clear. Solution and solid-state structural characterization of the protein in complex with a substrate analog revealed a highly unconventional H_2O_2-

activating distal environment with the reactive propionic acids (2 and 4) on the opposite side of the porphyrin plane. This suggested that, in contrast to direct C—H bond cleavage catalyzed by a high-valent iron intermediate, the coproheme oxidations must occur through mediating amino acid residues. A tyrosine that hydrogen bonds to propionate 2 in a position analogous to the substrate in ascorbate peroxidase is essential for both decarboxylations, while a lysine that salt bridges to propionate 4 is required solely for the second. A mechanism is proposed in which propionate 2 relays an oxidizing equivalent from a coproheme compound I intermediate to the reactive deprotonated tyrosine, forming Tyr$^•$. This residue then abstracts a net hydrogen atom (H$^•$) from propionate 2, followed by migration of the unpaired propionyl electron to the coproheme iron to yield the ferric harderoheme and CO_2 products. A similar pathway is proposed for decarboxylation of propionate 4, but with a lysine residue as an essential proton shuttle. The proposed reaction suggests an extended relay of heme-mediated e$^-$/H$^+$ transfers and a novel route for the conversion of carboxylic acids to alkenes.
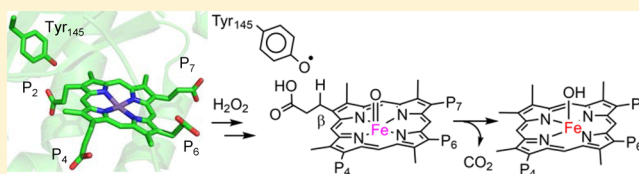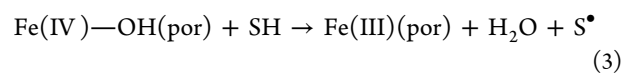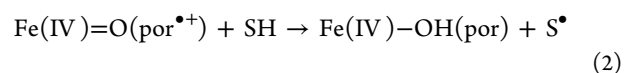
INTRODUCTION

Activation of O_2 or H_2O_2 by heme often leads to the generation of high-valent iron-oxo (ferryl) intermediates.[1] In reactions catalyzed by heme peroxidases, donation of two electrons from the Fe(III)-porphyrin complex results in heterolytic cleavage of the HO—OH bond. The resulting compound I intermediate carries one oxidizing equivalent on the iron and the other in the porphyrin π system, and is consequently described as Fe(IV)=O coupled to a porphyrin radical cation (por$^{•+}$):[2,3]

$$\text{Fe(III)por} + H_2O_2 \rightarrow \text{Fe(IV)=O(por}^{•+}) + H_2O \qquad (1)$$
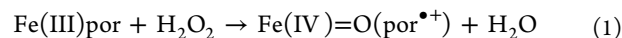
How this central intermediate forms and how it oxidizes compounds, sometimes over long distances, are longstanding questions in catalysis research. In reactions catalyzed by many cytochrome P450s and peroxidases,[4] 1 e$^-$ + 1 H$^+$ are transferred from a substrate to compound I. Such reactions, known as proton coupled electron transfers,[5] can occur in a single concerted proton/electron transfer step. Alternatively, as in the catalytic model for P450s,[3] the proton may migrate to the ferryl oxygen while the electron enters an orbital that is porphyrin-based. The overall reaction is described as hydrogen atom transfer.[6]

The proton and electron may have distinct routes to their separate destinations, though in only few cases have these been rigorously described. In ascorbate peroxidase (APX), the ascorbate substrate binds near and donates a hydrogen bond (H-bond) to one of the heme propionates (Figure S1 of the Supporting Information).[7,8] Hydrogen atom transfer from ascorbate, in both APX and a synthetic heme complex designed to mimic it,[9] is thought to occur with the propionate acting both as a base toward the proton and as the conduit for the electron to por$^{•+}$. Evidence further suggests that the proton is shuttled to an active site arginine and water molecules before finally arriving at the ferryl oxygen,[10] and the resulting Fe(IV)=O + H$^+$ or Fe(IV)—OH complex is known as compound II.[11] Transfer of a hydrogen atom from a second substrate leads back to the ferric heme and a molecule of water. Representing the substrate as SH gives the general reaction scheme:

$$\text{Fe(IV)=O(por}^{•+}) + SH \rightarrow \text{Fe(IV)—OH(por)} + S^• \qquad (2)$$

$$\text{Fe(IV)—OH(por)} + SH \rightarrow \text{Fe(III)(por)} + H_2O + S^• \qquad (3)$$

The propionate in APX (Figure S1) allows the heme to transmit oxidizing equivalents, from the site where the heme iron converts H_2O_2 to its catalytically activated compound I form, to the substrate binding site. In some peroxidases, including cytochrome c peroxidase (CCP) and lignin peroxidase (LnP),[12−14] the sites of heme-Fe(III)/H_2O_2 reaction and substrate oxidation may be quite spatially remote. Redox-active amino acid side chains[15−17] in addition to the propionates[18] act as internal mediators within these enzymes. These supply the means to move oxidizing equivalents away from por$^{\bullet+}$ and to the site where substrates bind, greatly extending the catalytic reach of heme as an oxidation catalyst.

Here, we describe the combined structural and solution-state characterization of a H_2O_2-activating heme protein in which the iron and the pair of organic substrates have an unusual spatial and electronic relationship. The enzyme uses H_2O_2 as an oxidant in the successive decarboxylations of propionates 2 and 4 of iron coproporphyrin III (coproheme), which serves as both substrate and cofactor in the reactions (Scheme 1). Use of

Scheme 1. Reaction Catalyzed by Coproheme Decarboxylase[a]
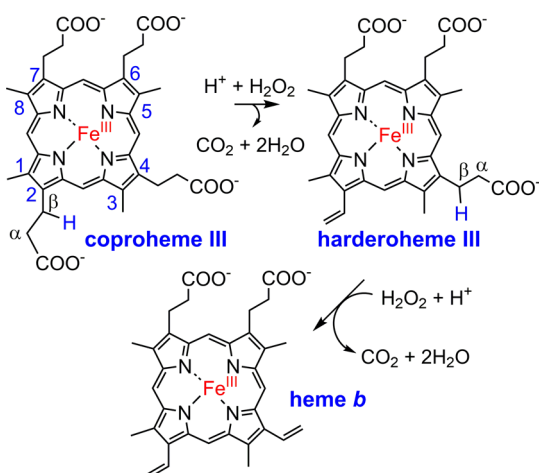
[a]Net loss of 2e$^-$ + H$^+$ from the Cα—Cβ bond of each propionate occurs along with decarboxylation. Involvement of Fe(III), H_2O_2, and harderoheme III in the reaction scheme was previously verified.[21,22] The porphyrin species are drawn in their expected protonation states at pH 7.

H_2O_2 as the biological oxidant in a decarboxylation or indeed any C—C bond cleavage is a highly uncommon feature of this enzyme,[19] which is encoded by the *hemQ* gene and which is responsible for the last step in heme biosynthesis in many Gram-positive bacteria.[20] The 1.8 Å resolution structure of the protein in complex with its Mn(III)-containing substrate analog clearly shows the two reactive propionates residing below (on the proximal side of) the coproheme plane, in a position where they cannot directly make contact with a ferryl intermediate. Instead, the structure suggests and the solution data support an electron/proton relay involving the heme, its propionates, and reactive amino acid side chains, leading to net transfers of an electron and a hydrogen atom from the reactive propionates themselves. The structurally inferred, experimentally supported reaction mechanism is unprecedented in biology. As such, it suggests possible new avenues for extending the catalytic repertoire of synthetic heme complexes.

■ EXPERIMENTAL SECTION

Expression, Purification, and Ligand Binding to WT and Mutant Coproheme Decarboxylases. The sequence of the protein encoded by the *hemQ* from *Geobacillus stearothermophilus* (*Gs*, NCBI accession WP_053414189, PDB ID: 1T0T)[23] was used to design a codon-optimized synthetic *hemQ* gene for expression in untagged form in *Escherichia coli*. The gene was inserted into a pET14(a) plasmid between the Nde1 and Xho1 restriction sites and used to transform competent *E. coli* Tuner (DE3) cells (Novagen). A similar construct for expressing the untagged, homologous protein from *Staphylococcus aureus* (*Sa*) was previously described.[21] A QuikChange Lightning Site-Directed Mutagenesis Kit (Agilent) was used to generate site-directed mutants of *Sa* decarboxylase using the manufacturer's instructions and primers in Table S1. For residues closer to the protein interior, substitutions were made from Tyr/Ser, or Trp/Phe- in order to retain the hydrophobic/hydrophilic character of the WT residue while dramatically changing its size or chemical functionality. Residues at the solvent interface were substituted by Ala.

Proteins were overexpressed and isolated at >95% purity by reverse-anion exchange and gel filtration chromatography as previously described.[21] Concentrated proteins (Amicon, 10 000 MWCO centrifuge filters) were incubated in the dark with gentle stirring at 4 °C for 24 h with either the substrate ferric coproheme III or the substrate analog Mn(III) coproporphyrinate III (coproporphyrinate III = *tetrakis*-2,4,6,7-propionate-protoporphyrin, Frontier Scientific) in a 1:1 subunit:coproheme ratio. Unbound coproheme was removed and the protein−ligand complexes further purified on an S-200 Sephacryl gel filtration column (0.4 mL/min). Fractions were collected using an AKTA purification system and then screened via UV/vis spectroscopy (Cary50) for coproheme content. Fractions with R_z values ≥0.8 (R_z = absorbance$_{Soret}$/absorbance$_{280}$) were pooled. The Bradford and pyridine hemochrome assays for protein and released coproheme, respectively, were used to determine the coproheme occupancy in the purified complexes. Extinction coefficients determined for the *Gs* coproheme decarboxylase complexes were ε_{Soret} =110.6 mM^{-1} cm^{-1} (Fe-coproheme)[21] and ε_{Soret} =69.7 ± 6.6 mM^{-1} cm^{-1} (Mn−coproheme) (Figure S2).

Structure Determination. The *Gs* decarboxylase in complex with Mn(III)coproheme was crystallized by hanging drop vapor diffusion at 20 °C. Drops were assembled by mixing the complex (7 mg/mL in 10 mM HEPES-NaOH pH 7.5) with an equal volume of reservoir solution (0.1 M citrate pH 5.0−5.5, 15−25% (w/v) polyethylene glycol 3350). Bright red crystals of the complex formed after approximately 2 weeks. Crystals were briefly soaked in reservoir solution supplemented with 15% (w/v) glycerol as a cryoprotectant prior to freezing in liquid N_2. An X-ray diffraction data set to 1.8 Å was measured at Stanford Synchrotron Radiation Lightsource beamline 14−1 and processed with autoxds.[24] The structure was determined by molecular replacement using Phaser[25] in the CCP4 program suite.[26] Phaser was supplied with the nonsubstrate bound structure as a search model (PDB ID 1T0T). Model building and refinement and was done using Coot[26] and Phenix.[27] Electron density maps of the Phaser solution showed the presence of a ligand adjacent to His172 (*Sa* sequence numbering, Figure S3); Mn-coproheme (designated as 76R in the PDB file) was modeled into this electron density. Iterative rounds of model building with Coot and refinement with Phenix[24] yielded the final model (PDB ID 5T2K) with R_{free} = 17.6% and R_{work} = 15.4%. The following residues are not included in the final model due to weak electron density: residues 115−123, 114−117, 112−117, 114−119 and 115−123 (all *Gs* numbering) in subunits A, B C, D, and E, respectively. Molecular graphics were created with PyMOL (www.pymol.org).

Determining Protein-Heme Dissociation Constants. Values of K_D for equilibrium binding of decarboxylases/hemes were determined by fluorescence quenching (Cary). Tryptophan fluorescence (5 μM subunit) was excited at 295 nm and emission monitored at 340 nm. Quenched emission at 340 nm was plotted versus the concentration of added heme ligand. Plots were fitted with the Langmuir-Hill equation to determine the K_D.

$$\theta = \frac{[L]^n}{K_D + [L]^n} \tag{4}$$

where θ is the fraction of ligand-binding sites occupied by the ligand, $[L]$ is the free (unbound) ligand concentration, and n is the Hill coefficient describing cooperativity.

Reactions of Decarboxylase−Coproheme Complexes Monitored Following Titrimetric Addition of Oxidants. Complexes of decarboxylase with Mn− or Fe−coproheme (pH 7.4, 20 °C) were mixed with aliquots of H_2O_2 or peracetic acid from 1 to 50 mM stocks. The progress of reactions was monitored by UV/vis spectroscopy (Cary50, samples 10 μM in heme species). Reaction products were analyzed by high performance liquid chromatography (HPLC) and HPLC coupled to electrospray ionization mass spectrometry (HPLC-ESI-MS) (samples 40 μM in the heme species). MS was used to verify the identities of all reactants and products via their exact masses. Fe-bound coproheme, harderoheme (isomers III or IV), and heme *b*, or Mn-bound coproheme/heme *b* were separated and quantified via their integrated HPLC peak intensities referenced to standard curves.

HPLC 20 μL samples were injected onto a Hypersil Gold PFP 5 μm column (150 × 4.6 mm^2, Thermo Fisher) attached to an Agillent1100 series instrument. Solvent A was H_2O with 0.1% trifluoroacetic acid (TFA) and Solvent B was acetonitrile (ACN) with 0.1% TFA. Samples were run at a flow rate of 2 mL/min starting with isocratic 70% A:30% B for 3 min, followed by a linear gradient transitioning from 70% A to 5% A over 12 min. This was followed by isocratic 5% A for 5 min and a final isocratic run of 30% A for 3 min. UV/vis detection was at 411 nm. Standard curves ranging from 0−500 pmol of the tetrapyrroles versus peak areas were constructed. HPLC peak areas were determined in triplicate and error bars are reported as ±1 standard deviation.

HPLC-ESI-MS: The chromatography conditions described above were used with an Agilent PLRP-S PSDVB column (PL1312−1300) and 1290 HPLC system. Mass spectra were obtained on an Agilent 6538 quadrupole time-of-flight (QTOF) instrument with ESI source (drying gas 8.0 L/min, drying gas heat at 350 °C, nebulizer 55 psi, capillary voltage 3500 V, capillary exit 100 V). Spectra were collected in negative mode from 50 to 1700 m/z at a rate of 2 Hz.

Steady State Kinetics of Catalase Reactions. The conversion of H_2O_2 to O_2 and water by various decarboxylase-metalloporphyrin complexes was monitored continuously over time via polarography using a Clark O_2 electrode (YSI). The electrode was equilibrated to 20 °C for 1 h using a circulating water bath and calibrated to the concentration of O_2 in air-saturated distilled/deionized water. Reactions were carried out in 2 mL volumes (50 mM potassium phosphate buffer, pH 7.4) with 4 μM of enzyme-porphyrin complex and initiated by addition of 10−100 mM H_2O_2 stocks via airtight syringe (5−20 μL). Linear initial rates (v_i) were fit by least-squares regression to the first 5−10% of the progress of reaction curves (Kaleidagraph). Plots of v_i versus H_2O_2 concentration were fit to the Michaelis Menton equation:

$$\frac{v}{E} = \frac{k_{cat}[H_2O_2]}{K_m + [H_2O_2]} \tag{5}$$

Here, E is the concentration of enzyme-metalloporphyrin complex. Unreacted H_2O_2 was quantified at the end of reactions using horseradish peroxidase (HRP) and a colorimetric substrate (2,2′-Azinobis [3-ethylbenzothiazoline-6-sulfonic acid]-diammonium salt, ABTS). 0.5U/mL HRP and 500 μM ABTS (final concentrations) were added to the samples and incubated (25 °C) for 1 h. The absorbance at 738 nm was recorded and compared with a standard curve generated over 5−100 μM H_2O_2.

Resonance Raman (rR) Spectroscopy. Ferric samples for rR experiments were prepared at 25 to 60 μM coproheme-decarboxylase complex in 100 mM sodium phosphate at pH 7.5 Using Schlenk techniques, ferrous complexes were prepared anaerobically at 20 °C from ferric enzymes by reduction with an excess of buffered sodium dithionite. The CO complexes were prepared by flushing the ferrous enzymes with natural abundance CO or ^{13}CO (99% ^{13}C).

The rR spectra were recorded using the 135° backscattering geometry and f1 collection using a previously described spectrometer.[21] Either the 406.7 nm or the 413.1 nm emission line from a Kr$^+$ laser was used for Raman excitation with the laser beam focused to a line on a spinning 5 mm NMR tube. External spectral calibration standards for the rR spectra were toluene, acetone, methylene bromide, and d^6-dimethyl sulfoxide. Laser power for ferric samples ranged from 4 to 12 mW; ferrous CO complexes required laser irradiation powers of 1 to 3 mW to prevent CO photolysis. To check the integrity of the rR samples, their UV/visible spectra were checked before and after irradiation in the laser beam. Normal mode assignments were made by analogy to other heme proteins. Peak fitting analyses of the rR spectra were based on the minimum number of peaks required to achieve statistically valid fits of the spectra. Band shapes were assumed to be Gaussian and were well modeled by Gaussian line-shape functions.

■ RESULTS

Co-Crystals of the Decarboxylase with Mn−Coproheme Diffracted to 1.8 Å Resolution. Our ongoing biochemical characterization of the coproheme decarboxylase and its genetic knock out has focused on *S. aureus* due to the importance of pathogenic strains of that species.[21,28] Robotic screening of thousands of crystallization conditions failed to generate diffraction-quality crystals of the enzyme from *Sa*, either alone or in complex with metalloporphyrins. However, the substrate-free structure of a coproheme decarboxylase from another member of its phylum, *Geobacillus stearothermophilus*, was available through a structural genomics consortium (PDB ID: 1T0T).[23] The *Gs* and *Sa* proteins have 59% sequence identity (Figure S3). UV/visible and rR spectra (Figures S4 and S5) and reactivity (Figure S5) for the two are similar, though the *Gs* enzyme appears to require more H_2O_2 to convert bound coproheme or harderoheme to heme *b*, and the heme *b* complex with the protein is less stable (reflected in its higher K_D, Table S2). The lower protein/heme *b* affinity for the *Gs* decarboxylase may be responsible for the increased susceptibility of the heme *b* to degradation by H_2O_2, apparent in the H_2O_2 titration data shown in Figure S5. Given the overall similarity between the *Sa* and *Gs* proteins, we therefore attempted to generate crystals with Fe(III)coproheme using the *Gs* decarboxylase, which was likewise unsuccessful. The enzyme complex with the substrate analog Mn(III)coproheme, however, yielded large crystals that diffracted to 1.8 Å resolution (Table S3). In solution, neither the *Gs* nor the *Sa* Mn(III)coproheme-decarboxylase complex reacted with H_2O_2 (up to 50 equiv). However, the Mn(III) complexes reacted with peracetic acid (PAA), yielding the expected Mn-substituted harderoheme intermediate and heme *b* products (Figure S6).[22] These results suggest that the Mn(III)-coproheme binds in the catalytic orientation but is incapable of activating H_2O_2 and therefore is stable as a solid state complex in the presence of O_2 and ionizing X-ray radiation, conditions under which H_2O_2 may be spontaneously produced.

Structural Changes Associated with Substrate Binding to Coproheme Decarboxylase are Confined to the C-Terminus. Like other members of its family (Pfam 06778, which includes both chlorite dismutase [Cld] and coproheme decarboxylase enzymes),[29] the crystal structure of the *Gs* coproheme decarboxylase is a homopentamer where each subunit consists of two ferrodoxin-like α/β domains connected by a pseudo-2-fold axis (Figure 1A). The same domain is shared by both noncanonical IsdG-type heme oxygenases and heme-binding DyP-type peroxidases, as previously noted.[28,30]
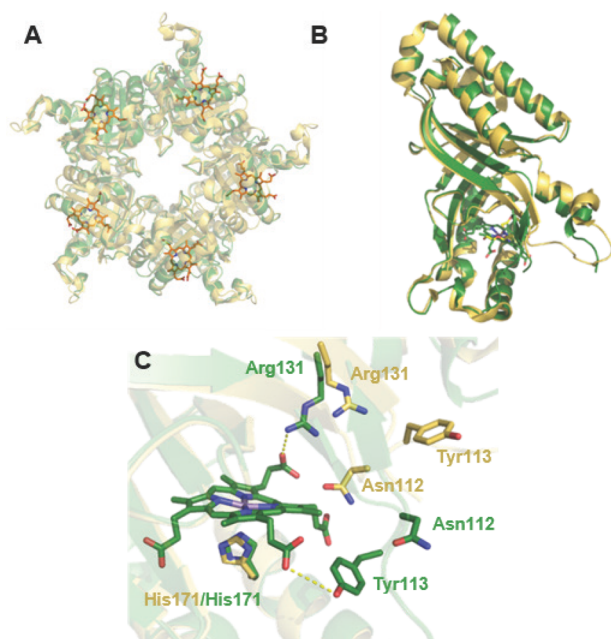
Figure 1. Superposition of the apo and ligand-bound forms of coproheme decarboxylase illustrate the effects of tetrapyrrole binding. A. The Mn(III)−coproporphyrin-bound decarboxylase homopentamer is shown in green with the bound Mn(III)−coproporphyrin ligands as sticks (orange) (5T2K) and the ligand-free structure in yellow (1T0T). The view is down the pseudo-C_5 axis with the coproheme-containing domains oriented toward the viewer. B. Superimposition of an individual subunit of coproheme decarboxylase in the apo (yellow) and ligand-bound (green) forms. Differences are localized around a flexible loop near residues 111−120 and the Mn(III)−coproporphyrin binding site. C. Close-up view of the Mn(III)-coproporphyrin binding site, illustrating prominent shifts in the positions of side chains for Asn112, Tyr113, and Arg131 in the apo- (yellow) and ligand-bound (green) forms.

The superimposed structures of the ligand-free (PDB ID 1T0T)[23] and -bound (5T2K) forms of subunit A are shown in Figure 1B ($C\alpha$ RMSD = 0.47 Å). The peptide backbone and side chains mostly overlay, with the structural changes accompanying ligand binding confined to the C-terminal region housing the Mn-coproheme. In particular, residues 111−121 form part of a loop on the solvent-exposed exterior of the ligand-free homopentamer, where they might constitute the site of substrate entry/product egress. (Sa residue numbering is used except where noted.) The most dramatic rearrangements in the ligand-bound structure occur here (Figure 1C). Though several of its side chains could not be modeled due to weak electron density in this region for the individual coproheme-bound subunits, the loop as a whole folds inward toward the coproheme in the ligand-bound structure. This rearrangement brings the side chain of Asn112, which occupies a position inside the substrate-binding pocket, toward the protein exterior in the ligand-bound structure. Tyr113 and Arg131, by contrast, form new contacts with propionates 4 and 6, respectively, which could be significant for the oxidative decarboxylation mechanism (see below).

Coproheme Binding Site Structure: Implications for Mechanism. The electron density map for Mn−coproheme bound to the active site (Figure 2A) illustrates the unambiguous assignment of the atomic positions of the porphyrin and all of its side chains in the crystal structure. The porphyrin ring is slightly ruffled, occupying roughly the same position as the molecule of solvent in the ligand-free structure or the heme b which serves as a cofactor in Clds. However, the coproheme is rotated approximately 90° about the pseudo-C_4 axis relative to the heme b in either Cld (Figure S7) or energy-minimized predictions of the structure of the decarboxylase−coproheme complex.[31] This orientation positions the two unreactive propionates (6 and 7, Scheme 1) pointing outward from the protein toward the solvent, where they occupy positions on the distal side of the heme plane (Figure 2B). The two reactive propionates (2 and 4), by contrast, are rotated to the proximal side of the porphyrin plane and well beyond the reach of the open, distal coordination site.

On the other side of the plane (proximal pocket), histidine 172 coordinates the Mn of the coproheme (2.3 Å) via the imidazole-N_ε atom (Figure 2B). The imidazole-N_δ is H-bonded to a water molecule, which is itself H-bonded to Ser222, Asp219, and the Met216 main chain carbonyl. Most H_2O_2-activating heme enzymes as well as Clds have an aspartic or glutamic acid as the hydrogen bonding donor in the analogous position,[32−34] leading to some degree of negative charge in the proximal ligand. The negatively charged histidine supplies an electronic push that favors heterolytic cleavage of the O—O bond in the heme-Fe(III)—OOH that forms in trans. Water is a comparatively weak H-bonding partner; consistent with previously reported rR spectra,[21] His172 is electronically neutral, leading to a more globin-like metal-His interaction.

The distal pocket (Figure 2C) is likewise distinct from other H_2O_2-reactive heme proteins. Canonical peroxidases share a distal histidine with a relatively low pKa due to a nearby arginine.[34] In its deprotonated form, the distal His acts as a base toward H_2O_2 (pKa = 11). Heterolytic bond cleavage in the resulting heme-Fe(III)—OOH complex is catalyzed by proton donation from the His-Arg pair, yielding Compound I and H_2O. By contrast, the distal environment in the coproheme decarboxylase is relatively hydrophobic. Ile187 hovers over the center of the porphyrin plane. Gln185 resides at its side and in the same sequence/structural position occupied by the distal arginine from Clds (Figure S8). This residue, which distinguishes the decarboxylase- and dismutase-encoding hemQ and cld genes, is important for the heme-dependent chlorite (ClO_2^-) decomposition mediated by Clds to yield Cl^- and O_2.[35]

At the edge of the distal pocket nearest the solvent interface, the Arg131 side chain sits at the center of a H-bonding network involving propionate 6, Gln185, and a water molecule (Figure 2C). This water occupies a position close to where the terminal oxygen of a coproheme-Fe(III)—OOH intermediate could reside. Though the solution pKa of the Arg side chain is high (12.5) and the propionate is low (3.2−3.5), the two together could in principle act as a base toward H_2O_2, an acid toward coproheme-Fe(III)—OOH, or both. An arginine side chain with a similar H-bond to a propionate has been proposed to act as a distal base in lieu of His-Arg in dye decoloring peroxidases.[36] Prior work showed that the second order reaction between the decarboxylase−coproheme complex and H_2O_2, which leads to the ferric heme b complex, accelerates with pH (~3-fold, pK_a = 7.4) and is solvent-isotope dependent (average $k(H_2O):k(D_2O) = 2.2$).[22] Both results suggest the involvement of proton movement in the rate limiting step of the H_2O_2 reaction. However, pH has a much larger influence over the analogous, acid−base-catalyzed steps in heme peroxidases.[34,37] The roles of these residues and of pH therefore remain to be determined.
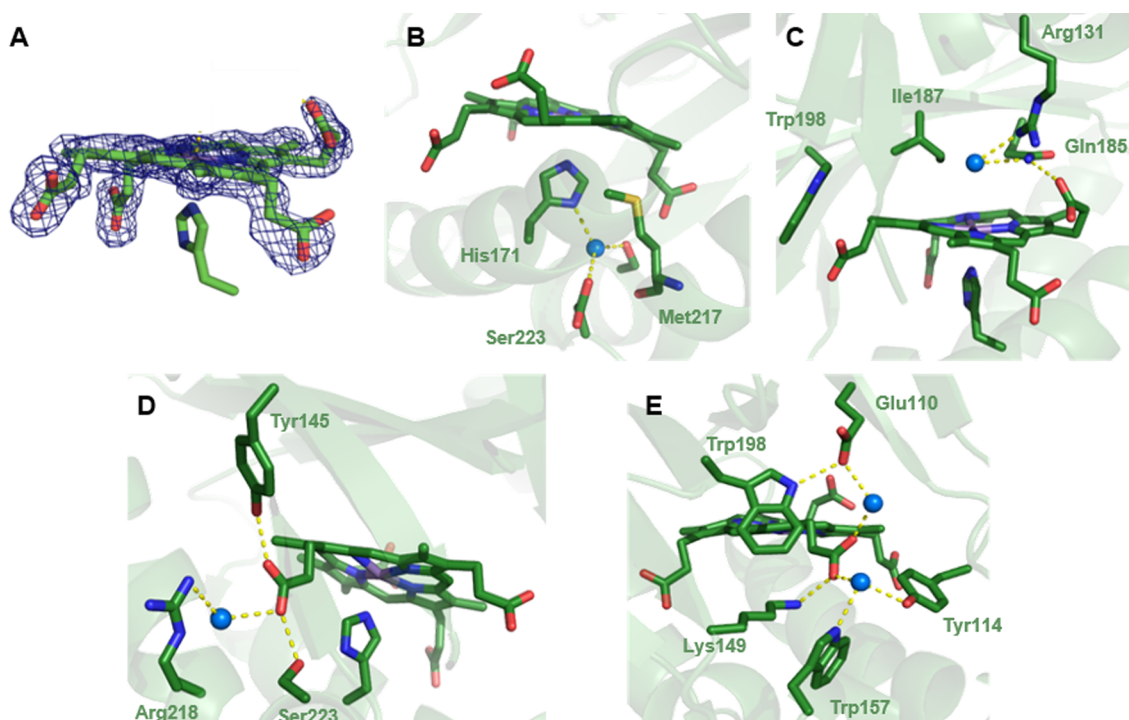
Figure 2. Structure of the coproheme binding site in coproheme decarboxylase has important implications for the chemical mechanism. A. View of the Mn–coproheme in subunit B with $Fo-Fc$ omit electron density map contoured at 3σ. B. The tetrapyrrole is slightly ruffled, with the two reactive propionates (2 and 4) below its approximate plane. A close-up view of the His171 ligand in the (proximal) pocket beneath the substrate analog shows that it binds to the metal through the imidazole–N_ε. The imidazole–N_δ forms an apparent hydrogen bond to a water molecule, which is itself hydrogen bonded to Ser223 and Asp220. C. The distal region above the coproheme plane is shown, highlighting the pair of unreactive propionates. The R131 side chain is part of a hydrogen bonding network involving propionate 6, Gln185, and a water molecule that occupies a position close to where the terminal oxygen of Fe–OOH might reside. The residue immediately over the coproheme plane is Ile187. The environment surrounding the reactive propionates 2 and 4 is shown in D and E, respectively.

Reactive propionates 2 and 4 are each converted (net $2e^- + 1H^+$ lost per propionate) to a vinyl group and CO_2 by a H_2O_2-mediated oxidation reaction (Scheme 1). Key residues surrounding each are shown in Figures 2D,E. Propionate 2, which reacts first,[21,22] forms H-bonds to the side chain hydroxyls of Ser223 (2.2 Å) and Tyr145 (2.8 Å). The former is part of a H-bonding network leading to the proximal His172. The latter is just 3.1 Å away from the C_β of the propionate (Scheme 1).

This was the observed site of net hydrogen atom removal catalyzed by coproporphyrinogen oxidase,[38] an enzyme that carries out analogous oxidative decarboxylations on the metal-free, reduced analog of coproheme III. Removal of a hydrogen atom at this position leaves a carbon radical conjugated to, and consequently stabilized by, the tetrapyrrole. Additionally, propionate 2 is H-bonded to a water molecule which is in turn H-bonded to Arg218. Propionate 4 is directly H-bonded/salt-bridged to Lys149 (2.7 Å), and indirectly to Trp156 and Tyr113 by a network of H-bonds including a bridging water molecule. Another H-bond network leads to Trp198 via the $O_{\varepsilon 1}$ atom of Glu109 and a second water molecule. The N_ε of Trp198 has the closest through-space approach to the C_β of propionate 4 (3.9 Å). The occurrence of multiple residues with possible redox (Tyr, Trp) and proton-translocating activities suggests one or more may be involved in catalyzing the two oxidative decarboxylations.

The solution state Sa and Gs decarboxylase heme environments are similar to one another and distinct from chlorite dismutases. Resonance Raman spectra were measured for the Sa and Gs decarboxylases in complex with ferric coproheme and heme b (Figure 3A). Comparison of the low frequency spectra of the coproheme complexes demonstrated similarities in their propionate bending ($\delta(C_\beta C_c C_d)$ (in this nomenclature C_c and C_d correspond to carbon atoms labeled C_β and C_α in Scheme 1) (Sa: 374 and 393 cm^{-1}; Gs: 374 and 395 cm^{-1}). Reaction of both coproheme–decarboxylase complexes with H_2O_2 (Figure S3) yielded comparable rR spectral changes,[21] including the appearance of bands corresponding to vinyl stretching and bending modes with very similar frequencies (1627 and 415–418 cm^{-1}, respectively). The 374 cm^{-1} propionate bending frequency is unaffected by decarboxylation while the second propionate bending frequency decreases by 4 cm^{-1} in both decarboxylases. The similarities between the solution spectra and reactivities of the Gs and Sa enzyme–substrate complexes suggest it is reasonable to expect that their structures, especially the positioning of their reactive coproheme 2- and 4-propionate groups, are comparable.

Prior simulations of coproheme binding to the decarboxylase had the nonreactive propionates 6 and 7 in the same positions as the propionates of the heme b in the Cld structures, in contrast with the solid state structure shown here.[31] Unique peripheral substituent environments of ferric heme b in decarboxylases and Clds are supported by their propionate and vinyl ($\delta(C_\beta C_a C_b)$) bending mode frequencies. The decarboxylase complexes exhibit $\delta(C_\beta C_c C_d)$ and $\delta(C_\beta C_a C_b)$ frequencies 8–11 cm^{-1} and 4–8 cm^{-1} lower, respectively, relative to those modes in WT DaCld and DaCld Arg183Gln mutant (Figure 3A).[35] The latter substitution exchanges the
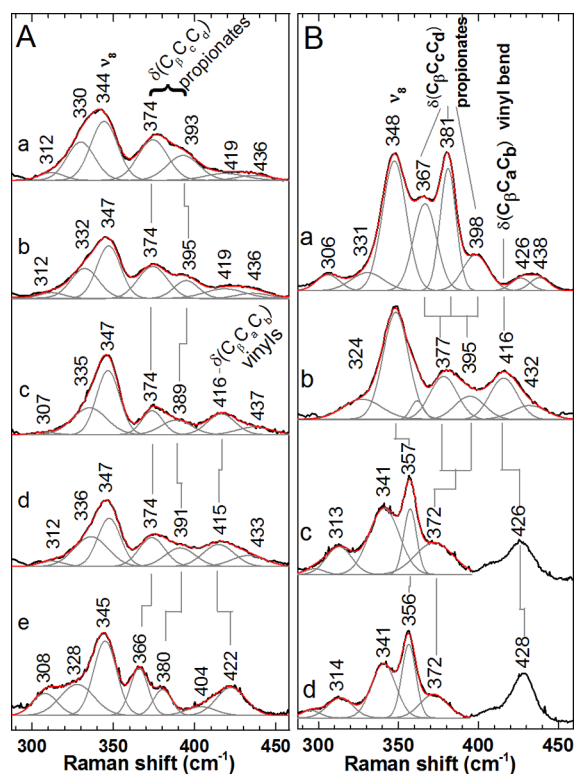
Figure 3. Low frequency rR spectra report on the core and peripheral environment of hemes bound to decarboxylases. (A) The 406.7 nm excited rR spectra of ferric forms of (a) coproheme:*Sa* decarboxylase, (b) coproheme:*Gs* decarboxylase, (c) heme *b*:*Sa* decarboxylase, (d) heme *b*:*Gs* decarboxylase, and (e) *Da*Cld(R183Q). Ferric samples were in 100 mM potassium phosphate at pH 7.4. (B) Soret-excited rR spectra of CO complexes of (a) coproheme:*Sa* decarboxylase, (b) heme *b*:*Sa* decarboxylase, (c) WT *Da*Cld, and (d) *Da*Cld(R183Q). Both *Da*Cld enzymes contain heme *b*. Spectra of CO samples in 100 mM potassium phosphate at pH 6.8 were acquired with 413.1 nm excitation and 2 mW power at the sample. Original spectra, black; fit spectra, red; component bands making up the fit spectra, gray.

Cld-associated distal Arg with the distal Gln of the *Sa* decarboxylase, rendering their distal environments more similar. To further examine the solution state environment of the nonreactive propionates, the rR spectrum for the ferrous *Sa* decarboxylase-heme *b* complex with CO was measured and compared with counterpart spectra from WT *Da*Cld and the *Da*Cld(R183Q) (Figure 3B). Comparison of the decarboxylase–CO and Cld–CO spectra clearly shows that the bands associated with propionate and vinyl bending, as well as the porphyrin ring, occur at different frequencies and with different band widths. The bending modes for propionates 6 and 7 of heme *b*:decarboxylase–CO are observed at 377 and 395 cm^{-1}, in contrast to one broad band at 372 cm^{-1} in the *Da*Cld-CO spectrum. The frequency of the vinyl bending mode for heme *b*:decarboxylase–CO is 10 cm^{-1} lower than that of WT *Da*Cld (416 versus 426 cm^{-1}). The *Da*Cld R183Q mutation has little effect on these propionate frequencies, suggesting that the observed differences in the spectra are not due to differences in their distal environments. In addition to these differences in vinyl/propionate-associated frequencies, the ν_8 core size marker band (symmetric M—N stretch) of the heme *b*:decarboxylase–CO occurs at 348 cm^{-1}, and 8–9 cm^{-1} higher in frequency in the *Da*Cld spectrum. Finally, a large band at 341 cm^{-1} that is tentatively assigned to the pyrrole tilting mode (γ_6) in *Da*Cld is

absent from the decarboxylase spectrum. These differences collectively reveal distinct peripheral and core heme conformations for the decarboxylases and Clds.

Solution-state spectroscopy indicates retention of the globin-like Fe-His bond but diminishing distal interactions as the propionates are oxidized. The ferrous heme–CO complex is a sensitive probe of heme coordination and the electrostatic character of its binding site inside proteins.[39–42] The CO complexes of the ferrous coproheme-, harderoheme-, and heme *b*-bound decarboxylase (*Sa*) were generated and their spectra analyzed for placement on a ν_{Fe-C}/ν_{C-O} correlation plot (Figure 4). Three isotope-sensitive (i.e., natural abundance CO, designated ^{12}CO, versus ^{13}CO) bands were detected for each of the aforementioned hemes. Based on their frequencies and isotope shifts, they were assigned to the Fe—C and C—O stretching (ν_{Fe-C} and ν_{C-O}) and FeCO bending (δ_{FeCO}) modes for CO-bound forms: coproheme, 513, 1941, and 582 cm^{-1}; harderoheme, 502, 1955, and 579 cm^{-1}; heme *b*, 498, 1958, and 577 cm^{-1}, respectively (Figure 4A). The same isotopically sensitive bands were observed for the heme *b*-CO, whether generated by binding ferric heme *b* to the enzyme or by the enzymatic action of the decarboxylase.

All of the CO complexes generated here fell on the inverse correlation line associated with charge-neutral proximal histidine ligands (Figure 4B), consistent with the proximal pocket structure, as revealed by x-ray crystallography, (Figure 2B) and with retention of the proximal histidine as the substrate converts to product. However, the location along the histidine correlation line for the three decarboxylase complexes varied, consistent with a changing distal environment. Stronger interactions of the CO ligand with positively charged or H-bond donating residues on the distal side of the heme lead to greater π back bonding and, therefore, to points higher on the imidazole line. The decarboxylase complex with coproheme is highest on the line, in a position consistent with moderate H-bond donation to or electrostatic interaction with the bound CO and the distal pocket. The harderoheme complex is much lower on the correlation line and close to the position of heme *b*, which is lowest of all. The loss of Fe—C π bonding character and increase in the C—O π bonding character in the three CO complexes is consistent with the progressive loss of distal interaction as the substrate is oxidized.

The positions of these complexes on the line can be further interpreted in terms of distal structure using available data from Clds. Two conformers, described as closed and open forms, have been reported for the pH 6.5 and 9 crystal structures of *Da*Cld as well as in rR spectra of *Da*Cld—CO.[45,46] These have the distal Arg183 oriented toward and away from the open coordination position above the heme plane, respectively. The coproheme:decarboxylase–CO is comparable to the closed form of *Da*Cld(Arg183Gln)–CO, suggesting similar distal environments. The closed form of WT *Da*Cld—CO, with its distal Arg, is higher up on the correlation line; as one would predict, the distal Arg interacts with the bound CO in a stronger manner than the distal Gln in either coproheme:decarboxylase–CO or *Da*Cld(Arg183Gln)-CO. The heme *b*:decarboxylase–CO falls at a position similar to the open form of *Da*Cld—CO and the CO complex of the Cld from *Candidatus Nitrospira defluvii*.[47] The degree of distal pocket interaction with the bound CO in these three complexes is similar and small.

Coproheme-Bound CO Interacts with the Conserved Distal Gln. The crystal structure suggests that Gln185 and/or
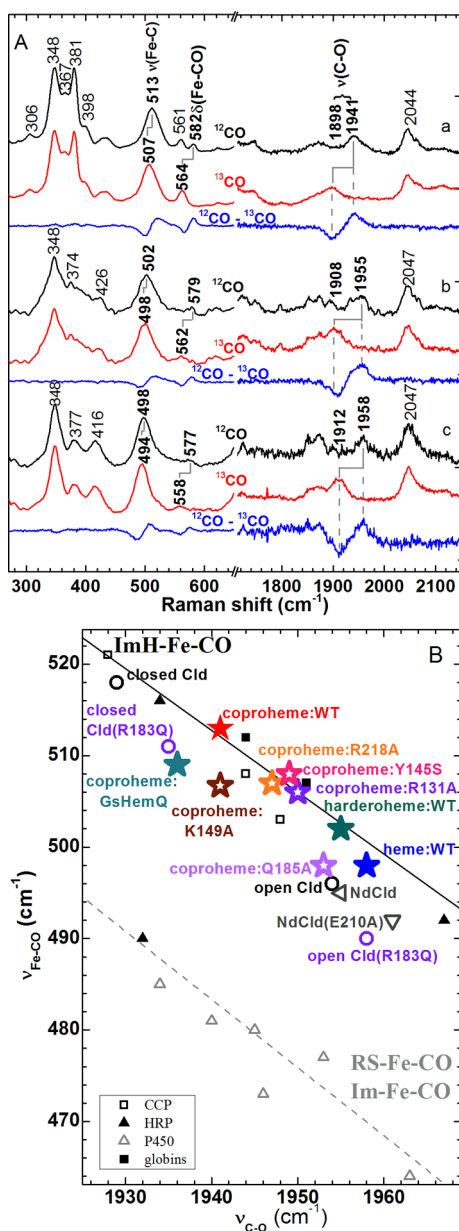
Figure 4. rR characterization of ferrous CO complexes of the *Sa* decarboxylase report on their proximal ligands and distal environments. (A) Soret-excited rR spectra of the isotopomers of CO complexes of the decarboxylase bound to (a) coproheme (b) harderoheme III, and (c) heme *b* at pH 6.8. Spectra were acquired with 413.1 nm excitation and 2 mW power at the sample. Natural abundance CO, (indicated by ^{12}CO) complex, black; ^{13}CO complex, red; difference spectra ^{12}CO—^{13}CO, blue. (B) Backbonding correlation plot of ν_{Fe-C} versus ν_{C-O} for ferrous carbonyls of heme proteins shows the dependences of their positions on axial ligation and distal pocket properties. The black line correlates ν_{Fe-C} with ν_{C-O} for six-coordinate Fe—CO adducts in which the sixth ligand is histidine (neutral imidazole). The gray dashed line represents six-coordinate Fe—CO adducts in which the sixth ligand is a thiolate or and imidazolate. Points used for these lines are tabulated in Table S1 of ref 43. Data for *Da*Clds and *Nd*Clds are from refs 43 and 44, respectively.

Arg131 could make contact with the terminal oxygen of a ferric coproheme−OOH complex. To examine this hypothesis, rR spectra for the ferrous coproheme−CO complexes were used to assess the distal environment sampled by a bound diatomic ligand inside the Gln185Ala and Arg131Ala variant decarbox-

ylases. The ν_{Fe-C} and ν_{C-O} frequencies for the Gln185Ala−CO complex (498 and 1953 cm^{-1}, respectively) (Figure S9) dramatically shift the Gln185Ala−CO point down the correlation line away from the WT coproheme complex and to a position close to the heme *b*-decarboxylase (Figure 4B.). This indicates loss of distal interaction when Gln185 is absent. The Arg131Ala−CO complex falls between WT and Gln185Ala on the ν_{Fe-C}/ ν_{C-O} correlation plot (Figures 4B and S8) indicating that this mutation has a smaller effect on the distal pocket interaction than Gln185Ala. Its distal environment is comparable to those observed for mutants in which H-bonds/ salt bridges to a propionate group have been disrupted (see below). This suggests that Arg131 plays a role at the periphery of the coproheme instead of in the distal pocket. Loss of the Arg charge could result in either a change in coproheme conformation because of loss of the interaction with propionate 6 or in an increase in solvent accessibility to the pocket. Either could be responsible for the characteristics of Arg131Ala-CO and its decreased activity with H_2O_2 described below. Consistent with these observations, the Gln185Ala but not the Arg131Ala exhibits impaired reactivity (described below).

Disruption of H-Bonding to Propionates 2 and 4 Alters Heme Conformation. The presence of H-bonds or salt bridges to propionates 2 (Tyr145, Arg218) and 4 (Lys149) are predicted by the structure (Figure 2). To test whether these apparent interactions modulate the electronic structure of the coproheme, the site-specific Tyr145Ser, Lys149Ala, and Arg218Ala mutants were generated. The rR spectra of these coproheme:mutant−CO complexes are compared in Figures 4B and S8 with their ν_{Fe-C} and ν_{C-O} frequencies given in Table S4. As judged by their position on the ν_{Fe-C}/ν_{C-O} correlation plot (Figure 4B), the mutant:coproheme−CO complexes, like WT coproheme−CO, retain the neutral His as the proximal ligand. The CO interactions with their distal environments, however, have been diminished. If the only role of the H-bonds/salt bridges to the reactive propionates is to position them for decarboxylation, then loss of these interactions would not be expected to change exogenous ligand interactions with the distal pocket. This result therefore argues that the roles of the H-bond donors to propionates 2 and 4 are more nuanced than simply positioning their carboxylate groups and the changes in their reactivity could be due, in part, to changes in the distal pocket interactions and/or distortions of the coproheme plane that direct the reactivity of the high-valent intermediate toward oxidative decarboxylation of propionate 2 or 4.

Three bands have been tentatively assigned to propionate bending modes in the CO complexes of WT, Tyr145Ser, Arg218Ala and Lys149Ala coproheme:decarboxylases (Figure S8B and Table S4). The Try145Ser mutant has a propionate bending band at 361 cm^{-1} that is 6 cm^{-1} lower than the comparable $\delta(C_\beta C_c C_d)$ band in the WT CO complex; the other two $\delta(C_\beta C_c C_d)$ frequencies are unaffected indicating that the band at 367 cm^{-1} in the WT CO spectrum is due to propionate 2. Loss of the Try145 H-bond to propionate 2 results in a significant alteration in its environment. In contrast, all three bands assigned to the propionate bending modes in Arg218Ala and Lys149Ala CO complexes exhibit decreases of 3 cm^{-1} in their frequencies of relative to WT. This indicates that disruption of the H-bond network between propionate 2 and Arg218 or the salt bridge between Lys149 and propionate 4 lead to more global changes in coproheme environment than the very localized effect of Tyr145 mutation. Interestingly, the

ν_8 band, a core size marker band that reports Fe—N$_{pyrrole}$ stretching, exhibits a decrease in frequency for all three mutants. This is consistent with increases in the porphyrin core size upon mutation of the amino acids that interact with the reactive propionates 2 and 4. These features suggest that the interaction of these residues with the coroheme are important in determining the degree to which the heme conformation deviates from planarity. Thus, stepwise changes in the heme planarity may contribute to the structural basis for regioselectivity in oxidizing propionates 2 and 4.

Tyr145 is essential for the decarboxylation of coroheme and harderoheme III; Lys149 contributes to decarboxylation of harderoheme III. On the basis of their proximity to the substrate and their catalytic roles in other enzymes, we hypothesized that several residues in Figure 2 may have essential roles in catalysis. We made a series of mutations in the *Sa* enzyme at a total of eight key positions, including those described above (Table S2). All of the mutants bound coroheme with >80% occupancy, with K_D values similar to WT and varying by less than an order of magnitude (Table S2, Figure S10−11). The catalytic competence of each mutant−coroheme complex was examined to determine which residues were essential for turnover, specifically whether each generated the expected intermediate (harderoheme III) and product (heme *b*) and how much oxidant was required.

The WT enzyme required 5 equiv of H$_2$O$_2$ to turn over 90% of the initially bound coroheme. Harderoheme III was the observed intermediate, maximizing after delivery of 2 equiv H$_2$O$_2$ (Figure S5) and fully converting to heme *b* with a total of 10−12 equiv of H$_2$O$_2$. Addition of further oxidant has been observed to bring about the complete degradation of the heme *b* chromophore.[21]

The most dramatic deviations from WT behavior were obtained for the Tyr145Ser and Lys149Ala mutants (Figure 5). Tyr145Ser, in which the H-bond to propionate 2 is eliminated, required ~3000 equiv of H$_2$O$_2$ to turn over ≥95% of the coroheme substrate (Table S2). Neither harderoheme III nor heme *b* appeared as intermediates or products. Instead, the coroheme degraded without detectable products. The Tyr145Ser mutant readily bound harderoheme so its catalytic competence toward this stable intermediate was investigated. Harderoheme-Tyr145Ser mutant did not form observable heme *b* upon reaction with H$_2$O$_2$ (Figure S12). The Lys149Ala mutant, in which the salt bridge to propionate 4 is removed, required ~300 equiv of H$_2$O$_2$ to turn over ≥95% of the substrate. However, the major product was harderoheme III, with relatively little turnover of this species to heme *b*. This suggests that Lys149 is essential specifically for the conversion of harderoheme to heme *b*, while Tyr145 appears to play a role in both decarboxylation reactions.

Substitutions of other potentially significant residues surrounding propionate 2 (Arg218Ala) or 4 (Tyr113Ser, Trp157Phe, Trp198Phe), or in the distal pocket (Gln185Ala, Arg131Ala) had far smaller effects, suggesting that none of these on its own is essential for catalysis. Instead, the Gln185Ala and Arg131Ala mutants brought about small increases in the amount of H$_2$O$_2$ required to effect substrate conversion (60 and 24 equiv, respectively). The Gln185Ala mutant additionally saw exhibited a marked decrease in the amount of harderoheme III accrued, suggesting this mutation had a proportionally greater impact on the first decarboxylation than the second. Arg218Ala, Trp157Phe, and Trp198Phe all behaved very similarly to WT, while the heme *b* product of
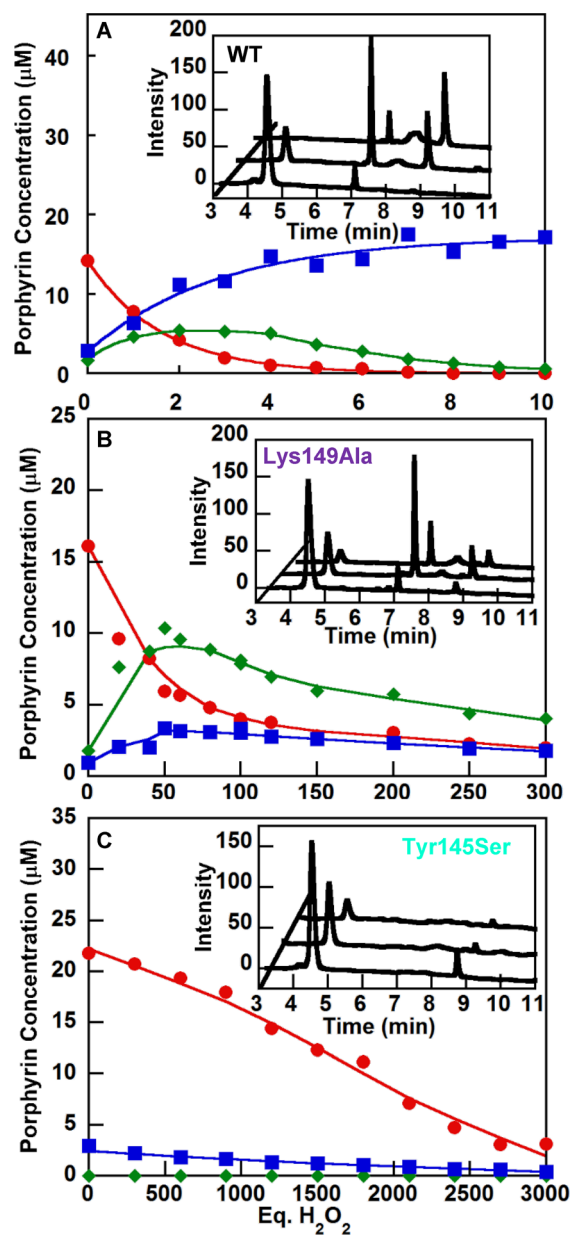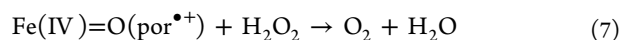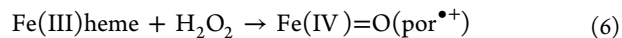

Figure 5. Mutations at Lys149 and Tyr145 prevent decarboxylation of one or both propionic acid substrates, respectively. Unreacted coroheme (red), harderoheme III intermediate (green), and the heme *b* product (blue) of the coroheme decarboxylase reaction with increasing equiv of H$_2$O$_2$ were quantified by HPLC for (top) WT enzyme and the mutants (center) Lys149Ala and (bottom) Tyr145Ser. HPLC traces illustrating the starting material, observable intermediates, and final products are shown as insets. Retention times for unreacted coroheme, the harderoheme III intermediate, and heme *b* product were 4.8, 7.1, and 8.9 min, respectively.

Tyr113Ser was slightly less stable toward H$_2$O$_2$, possibly due to weaker heme *b* binding (Figure S13).

The excess H$_2$O$_2$ required for coroheme turnover can be largely accounted for by catalase activity. The *Sa* decarboxylase containing heme *b* was previously shown to have catalase activity:

$$Fe(III)heme + H_2O_2 \rightarrow Fe(IV)=O(por^{\bullet+}) \qquad (6)$$

$$Fe(IV)=O(por^{\bullet+}) + H_2O_2 \rightarrow O_2 + H_2O \qquad (7)$$

This reaction (~50 turnovers) occurs concomitantly with heme *b* degradation.[28]

It is possible that some of the excess H_2O_2 required for coproheme conversion to heme *b* might be expended in the catalase reaction. Following addition of 12 equiv of H_2O_2 (120 μM) to the decarboxylase-coproheme complex (10 μM), one equiv of O_2 (10 μM) (measured by O_2 polarography) (Figure 6A) was generated over the same time frame in which
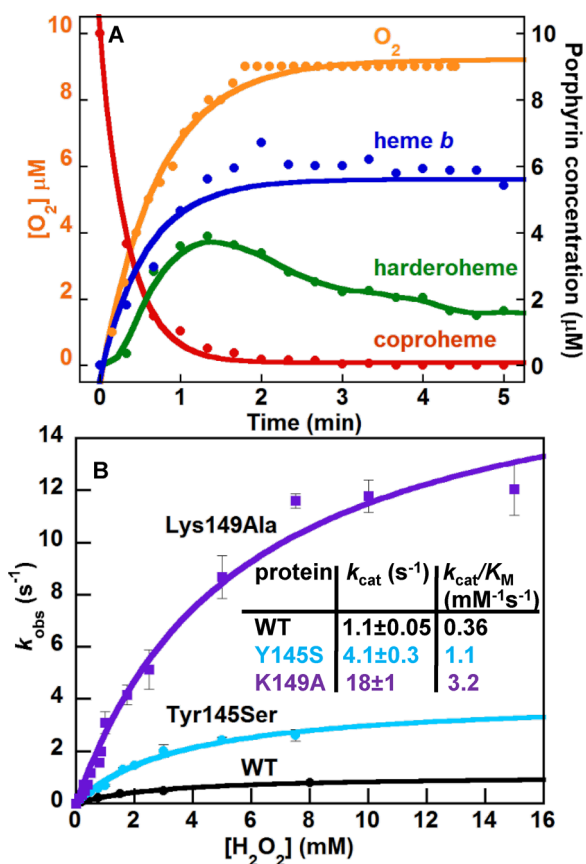

Figure 6. The catalase activity of coproheme decarboxylase is strongly enhanced in the Lys149Ala and Tyr145Ser mutants. (A) The progress of the coproheme decarboxylase reaction over time [coproheme (red), harderoheme III (green), heme *b* (blue)] measured previously[22] is shown superimposed on the time course for O_2 production (orange) (10 μM enzyme-coproheme, 120 μM H_2O_2, 50 mM KPi, pH 7.4, 25 °C). The generation of ~10 μM O_2 via the catalase reaction suggests that ~20 μM H_2O_2 was consumed during the same time window in which coproheme converted to heme *b*. (B) Initial rates of O_2 production were measured as a function of $[H_2O_2]$ and fit to eq 5 for the WT (black), Tyr145Ser (cyan), and Lys149Ala (purple) decarboxylases. The resulting steady state parameters describing catalase activity are tabulated in the inset.

coproheme converted to heme *b*. In light of the mechanism above, 2 equiv of H_2O_2 (likely not a physiologically relevant amount) can be accounted for via the catalase reaction, in addition to the 2 required for the decarboxylation reactions. The remaining 8 of the initial 12 equiv, though well within the limits of detection, were not detected by HRP-based colorimetric assays as the end of the reaction. Control reactions in which the ligand-free/apoprotein (5 μM) was mixed with 12 equiv H_2O_2 (60 μM) under the same conditions showed that ~8 equiv of H_2O_2 (40 μM) were consumed in a heme-independent reaction with the apoprotein without concomitant

production of O_2, while 4 equiv (22 μM) remained unreacted in solution (Figure S14).

The large excess of H_2O_2 required to turn over the coproheme bound to the Tyr149Ser and Lys145Ala mutants could likewise be primarily accounted for via the catalase reaction (Figure S15). Mutation of either residue increases the values of both k_{cat} and $k_{cat}/K_M(H_2O_2)$ relative to WT (Figure 6B). This suggests that either mutation stabilizes the heme species, thereby enhancing their efficiency as catalases.

■ DISCUSSION

Coproheme decarboxylase catalyzes H_2O_2-dependent C—C bond cleavage reactions to liberate two molecules CO_2 from a pair of propionic acids, converting each to a vinyl group (Scheme 1). An analogous reaction is catalyzed by the bacterial cytochrome P450, OleT.[48] Ferric OleT and H_2O_2 react to generate compound I, which in turn abstracts a hydrogen atom directly from the exogenous carboxylic acid substrate. Unique among P450s, this reaction is not followed by rebound between the substrate radical and Fe(IV)—OH.[19] Instead, the reaction is more peroxidase-like, with the unpaired electron from the nearby substrate reducing the iron to Fe(III), resulting in CO_2 and the alkene. A similar mechanism could be proposed for the coproheme decarboxylase, with the ferryl oxygen most likely interacting for steric reasons with the C_α—H of either propionate 2 or 4 (Scheme 1). However, the 1.8 Å structure of the enzyme in complex with its substrate analog (Figures 1 and 2) suggests two complications with any straightforward application of either the peroxidase or OleT model to the coproheme decarboxylase.

The first is that the apparatus for activating H_2O_2 found in most heme peroxidases, including CCP and APX (Figure S1 and Results),[12] is completely absent in the coproheme decarboxylase. The coproheme is instead ligated by an uncharged proximal His (Figures 2−4) and its open coordination position is flanked by a distal Gln. Both the Gln and the Arg to which it is connected via H-bonds through-water interact with a coproheme-bound CO. Although mutagenesis showed that neither Gln185 nor Arg131 was essential for catalysis, their interactions with bound CO suggests they could play activating roles toward H_2O_2. Some role for the protein is supported by prior studies of the reaction of the coproheme decarboxylase with peracetic acid: an oxygen atom donor that directly converts ferric hemes to Fe(IV) =O(por$^{•+}$) or Fe(IV)=O(Trp$^{•+}$) without the proton movement associated with H_2O_2.[22] The ferric coproheme decarboxylase reacts rapidly with peracetic acid to form the expected harderoheme intermediate and heme *b* product. The second order rate constant for the same reaction with H_2O_2 is 10-fold slower and, in contrast with the peracid reaction, dependent on both pH and solvent isotope (D_2O).[22] These observations strongly suggest that the reaction proceeds through a ferryl intermediate and that its formation is facilitated by protein-mediated proton transfers (Scheme 2A).

The second issue concerns the presumptive sites of substrate oxidation — the C_β—H bonds of propionic acids 2 and 4 — which the structure shows are spatially removed from the site of H_2O_2 activation at the metal. This separation immediately suggests that, in contrast with OleT, the reaction cannot proceed by direct interaction of a ferryl or other iron/oxygen intermediate with either propionate. A similar steric problem was noted previously in studies of mammalian peroxidases and some cytochrome P450s in which the methyl side chains of

Scheme 2. Proposed Mechanisms Consistent with the Available Data[a]
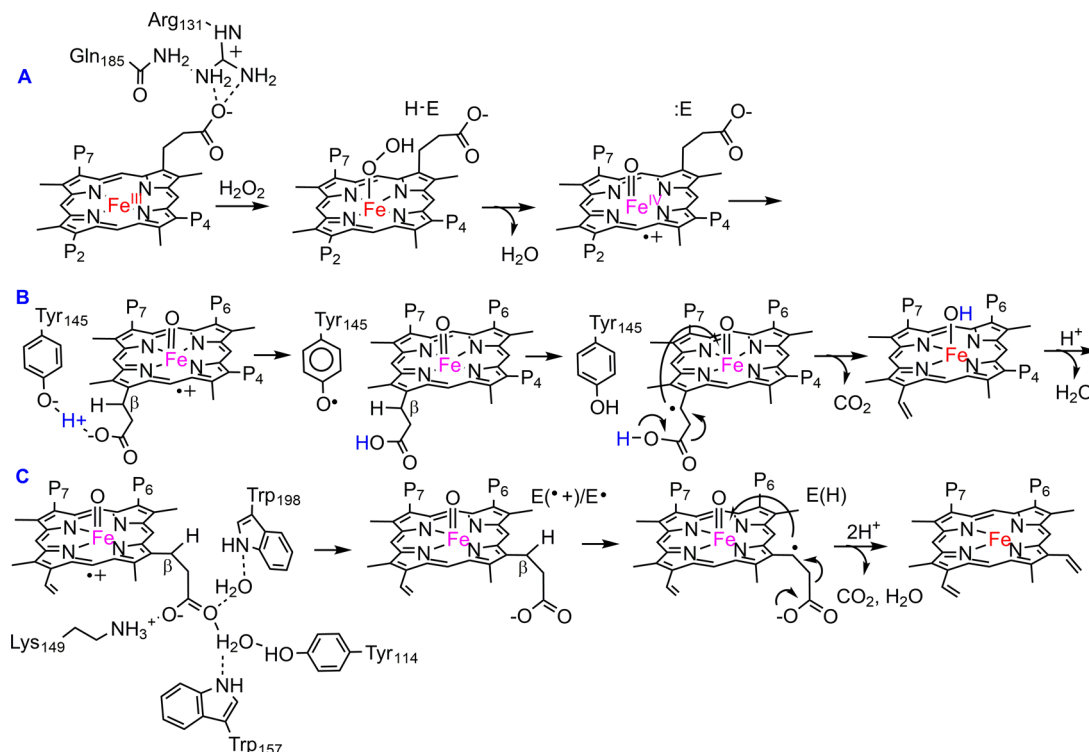
[a]A. Formation of Fe(IV) = O(coproporphyrin[•+]) (coproheme compound I) (E = enzyme; Fe(III) in red and Fe(IV) in purple). B. Oxidative decarboxylation of propionate 2 requires Tyr145. The neutral Tyr145-O[•] radical is depicted abstracting hydrogen (H[•]) from the propionate C_β, though this is hypothetical. Transfer of an electron and proton to the ferryl of Compound II then leads to the ferric—OH complex of harderoheme III, from which water can ultimately depart. C. Following another round of H_2O_2-activation analogous to (A), a second Fe(IV) = O(harderoporphyrin[•+]) complex forms. Three possible redox-active amino acids are connected to propionate 4 via hydrogen bonding through water molecules, though only Lys149 appeared to play a role decarboxylating propionate 4. The identity of the mediator for proton coupled electron transfer from the propionate (designated E[+•] or E[•]) is unclear. Net uptake of H[•] by the enzyme is designated via E(H).

heme b are oxidatively modified via a compound I intermediate. In each case, the steric relationships between the ferryl of compound I and the heme substituents imply the use of an amino acid side chain or multiple side chains as redox mediators.[49−51] Inspection of the environment surrounding propionate 2 (Figure 2C) immediately identified Tyr145 as a possible secondary site of oxidation following the initial generation of a coproheme compound I. The side chain of Tyr145 sits near to and forms an apparent H-bond with the carboxylate moiety of propionate 2, in a position analogous to the ascorbate binding site in APX (Figure S1).[8] This configuration suggested that Tyr145 might be well-positioned to be oxidized by the coproheme compound I (Scheme 2B), and that it may in fact act as the reactive species toward propionate 2. Consistent with that hypothesis, substitution of Tyr145 with Ser led to complete loss of coproheme decarboxylation. A concomitant large increase in catalase activity (Figure 6) suggested that, in the absence of Tyr145, the enzyme readily forms Fe(IV)=O(coproporphyrin[•+]) with the electron hole localized on the porphyrin.

Neutral tyrosyl radicals (TyrO[•]) are implicated in a variety of reactions, including those catalyzed by class I ribonucleotide reductase,[52] photosystem II,[53] galactose oxidase,[54] and prostaglandin-H synthase.[55] In each case, a metal center is involved in generating the tyrosyl radical, which then acts as the primary recipient of an electron or hydrogen atom from a substrate. In the case of prostaglandin-H synthase and other cyclooxygenases, the metal center is heme b, which oxidizes a

nearby tyrosine side chain via a compound I intermediate. The bond dissociation free energy associated with TyrO[•]/TyrOH in these systems as well as phenolic model compounds can be quite high[17,56] and, in the case of the tyrosine Z in photosystem II, thermodynamically sufficient for the oxidation of water. Net transfer of H[•] from the propionate C_β-H to Tyr145-O[•] would result in a resonance-stabilized coproheme propionyl-C_β radical, suggesting a proportionally lower requisite driving force for carrying out the reaction. Though mutagenesis showed it was not essential for coproheme turnover by the decarboxylase, the side chain of Arg218 is well-positioned to shuttle propionate-derived protons from the active site. A similarly situated arginine residue obligately serves this function in the oxidation of ascorbate by APX (Figure S1).[10] Transfer of a second electron from the $C_\beta^{•}$ through the porphyrin and to the coproheme Fe(IV) would result in the regeneration of Fe(III) and production of the vinyl and CO_2 (Scheme 2B).

Decarboxylation at propionate 2 is followed by a second, slightly faster[22] H_2O_2-dependent reaction at propionate 4. Inspection of the environment surrounding this group identified three readily oxidizable aromatic residues in its vicinity (Tyr114, Trp198, Trp157) as well as a lysine (Lys149) which, like Arg218, could potentially act as an initial recipient or conduit for protons (Figure 2E). Individual mutations at each of these residues showed that only Lys149 appeared to be essential for coproheme turnover. Substitution of this residue with alanine resulted in the accumulation of the three-propionate intermediate, harderoheme III (Scheme 1). This

result suggested that harderoheme maintains the same position as the coproheme substrate, as predicted by solution state rR, and loss of the harderoheme-Lys149 interaction specifically inhibits the decarboxylation of propionate 4.[22] We therefore conclude that H_2O_2 activation by the harderoheme-decarboxylase proceeds in a similar environment as the coproheme complex, though the Fe(III)/(II) reduction potential[22] and the degree of distal pocket interaction with the bound substrate (Figure 4) have diminished. The pronounced increase in catalase activity in the Lys149Ala mutant likewise suggests that it reacts with H_2O_2 to form Fe(IV)=O(harderoporphyrin$^{•+}$).

If this intermediate forms during catalytic turnover, then Tyr114, Trp198, and Trp157 all appear reasonably positioned to form Tyr-O$^•$ or Trp$^{•+}$ radicals by filling the electron hole on (harderoporphyrin$^{•+}$). The side chain could then mediate a reaction with propionate 4, where the C_β-H electron could migrate to the same (e.g., Tyr114-O$^•$) or separate destinations. In the latter case, Lys149 could serve an essential role as the proton acceptor in a proton coupled electron transfer. However, mutation of any of these aromatic residues independently had virtually no effect on the efficiency of either propionate decarboxylation. This suggests one of two interpretations. First, it is possible that radical density is spread over two or more of these residues, and that the others can compensate in the event that one is lost. Alternatively, Tyr145-O$^•$ could act as the enzyme's sole redox mediator toward both propionates 2 and 4.

Though the latter is farther from Tyr145, net proton coupled electron transfers can occur across long distances. The reactive Tyr-O$^•$ in ribonucleotide reductases sets an impressive precedent, reacting with a cysteine-SH over 35 Å away.[52] Supporting this hypothesis in part, we noted that reaction of the Tyr145Ser—coproheme complex with H_2O_2 yielded neither harderoheme nor heme *b*, suggesting that both decarboxylations are impaired by this substitution. Moreover, when a complex of the same mutant was prepared with exogenously supplied harderoheme III, its reaction with H_2O_2 also yielded no heme *b*. Tyr145 is clearly essential for both propionate oxidations, though whether it acts as a radical mediator in either case is still unknown. How Tyr145 would form the Tyr-O$^•$ radical in the absence of the conduit provided by propionate 2, once it has converted to vinyl, is an open question, though we note that there is a clear kinetic preference for oxidizing propionate 2 first. This oxidation could be facilitated by the existence of the propionate-Tyr145 interaction.

The chemistry, spectroscopy, and structure reported here constitute an internally consistent account of function and mechanism in this class of decarboxylases. Tyr145 and Lys149 are H-bonded to the reactive propionates 2 and 4, respectively, and play essential roles in the reactivity and regioselectivity of propionates 2 and 4 toward oxidation. These nonbonded interactions differ markedly from those recently reported for the *Listeria monocytogenes* enzyme (*Lm*HemQ), in which coproheme III is oriented such that propionates 2 and 7 are oriented toward the surface of the enzyme while propionates 4 and 6 are directed into the pocket. In the *Lm*HemQ structure, propionate 2 is H-bonded to Gln187, propionate 4 is H-bonded to Tyr147, and the unreactive propionate 6 is H-bonded to Lys151 (comparable to Gln185, Tyr145 and Lys149, respectively, in the *Sa* enzyme). Though there are some differences in crystallization parameters (*Gs* decarboxylase crystals were grown at pH 7.5, for example, whereas the *Lm* decarboxylase crystals were obtained at pH 9.0) the reasons for

this different coproheme orientation are unclear. Though it seems unlikely that homologous decarboxylases from different organisms would utilize different coproheme orientations, this possibility cannot be eliminated at this time. More in-depth comparison of the two coproheme-decarboxylase structures is not possible at the time of writing because the *Lm*HemQ structure has yet to be released.[57]

OleT and the coproheme decarboxylase described here are atypical for using H_2O_2 as the cosubstrate in an oxidative decarboxylation. Coproheme decarboxylase is further distinguished by its evident use of an extended relay of propionate and side chain mediators to convey electrons and protons away from its pair of substrates and toward H_2O_2, ultimately releasing CO_2. This use of the metalloporphyrin as a primary site of oxidation, in conjunction with a series of stably positioned mediators, also suggests an alternative approach for synthetic or semisynthetic catalysis of the oxidative decarboxylation of fatty acids to generate alkenes.

■ ASSOCIATED CONTENT

Ⓢ Supporting Information

The Supporting Information is available free of charge on the ACS Publications website at DOI: 10.1021/jacs.6b11324.

> Structure images, assays, spectra, binding constants, and analysis (15 data figures and 4 tables) (PDF)

■ AUTHOR INFORMATION

Corresponding Author

*jennifer.dubois1@montana.edu

ORCID Ⓘ

Jennifer L. DuBois: 0000-0001-5593-3391

Author Contributions

The manuscript was written through contributions of all authors. All authors have given approval to the final version of the manuscript.

Notes

The authors declare no competing financial interest.

■ ACKNOWLEDGMENTS

■ REFERENCES

(1) Traylor, T. G.; Traylor, P. S. Reactions of dioxygen and its reduced forms with heme proteins and model porphyrin complexes. In *Active Oxygen in Biochemistry*; Valentine, J. S.; Foote, C. S.; Greenberg, A.; Liebman, J. F., Eds.; Springer: Netherlands, 1995; pp 84−187.

(2) Dunford, H. B. *Heme Peroxidases*; Wiley-VCH: New York, 1999.

(3) Ortiz de Montellano, P. R. *Cytochrome P450: Structure, Mechanism and Biochemistry*, 3rd ed.; Kluwer Academic/Plenum: New York, 2005.

(4) Rittle, J.; Green, M. T. *Science* **2010**, *330*, 933−7.

(5) Hammes-Schiffer, S. *J. Am. Chem. Soc.* **2015**, *137*, 8860−8871.

(6) Reece, S. Y.; Hodgkiss, J. M.; Stubbe, J.; Nocera, D. G. *Philos. Trans. R. Soc., B* **2006**, *361*, 1351−1364.

(7) Macdonald, I. K.; Badyal, S. K.; Ghamsari, L.; Moody, P. C.; Raven, E. L. *Biochemistry* **2006**, *45*, 7808−7817.

(8) Sharp, K. H.; Mewies, M.; Moody, P. C.; Raven, E. L. *Nat. Struct. Biol.* **2003**, *10*, 303−307.

(9) Warren, J. J.; Mayer, J. M. *J. Am. Chem. Soc.* **2011**, *133*, 8544−8551.

(10) Efimov, I.; Badyal, S. K.; Metcalfe, C. L.; Macdonald, I.; Gumiero, A.; Raven, E. L.; Moody, P. C. *J. Am. Chem. Soc.* **2011**, *133*, 15376−15383.

(11) Gumiero, A.; Metcalfe, C. L.; Pearson, A. R.; Raven, E. L.; Moody, P. C. *J. Biol. Chem.* **2011**, *286*, 1260−1268.

(12) (a) Poulos, T. L. *Chem. Rev.* **2014**, *114*, 3919−3962. (b) Chreifi, G.; Baxter, E. L.; Doukov, T.; Cohen, A. E.; McPhillips, S. E.; Song, J.; Meharenna, Y. T.; Soltis, S. M.; Poulos, T. L. *Proc. Natl. Acad. Sci. U. S. A.* **2016**, *113*, 1226−1231.

(13) Pelletier, H.; Kraut, J. *Science* **1992**, *258*, 1748−1755.

(14) Choinowski, T.; Blodig, W.; Winterhalter, K. H.; Piontek, K. *J. Mol. Biol.* **1999**, *286*, 809−827.

(15) Colin, J.; Wiseman, B.; Switala, J.; Loewen, P.; Ivancich, A. *J. Am. Chem. Soc.* **2009**, *131*, 8557−8563.

(16) Sivaraja, M.; Goodin, D. B.; Smith, M.; Hoffman, B. M. *Science* **1989**, *245*, 738−740.

(17) Tommos, C.; Skalicky, J. J.; Pilloud, D. L.; Wand, A. J.; Dutton, P. L. *Biochemistry* **1999**, *38*, 9495−9507.

(18) Guallar, V. *J. Phys. Chem. B* **2008**, *112*, 13460−13464.

(19) Grant, J. L.; Mitchell, M. E.; Makris, T. M. *Proc. Natl. Acad. Sci. U. S. A.* **2016**, *113*, 10049−10054.

(20) Dailey, H.; Gerdes, S.; Dailey, T.; Burch, J.; Phillips, J. *Proc. Natl. Acad. Sci. U. S. A.* **2015**, *112*, 2210−2215.

(21) Celis, A. I.; Streit, B. R.; Moraski, G. C.; Kant, R.; Lash, T. D.; Lukat-Rodgers, G. S.; Rodgers, K. R.; DuBois, J. L. *Biochemistry* **2015**, *54*, 4022−4032.

(22) Streit, B. R.; Celis, A. I.; Shisler, K.; Rodgers, K. R.; Lukat-Rodgers, G. S.; DuBois, J. L. Reactions of ferrous coproheme decarboxylase (HemQ) with O_2 and H_2O_2 yield ferric heme b. Biochemistry. [Online early access]. Doi: 10.1021/acs.biochem.6b00958. Published online. Dec 5, 2016, http://pubs.acs.org/doi/abs/10.1021/acs.biochem.6b00958 (accessed Dec 12, 2016).

(23) Gilski, M.; Borek, D.; Chen, Y.; Collart, F.; Joachimiak, A.; Otwinowski, Z. RCSB Protein Data Bank http://www.rcsb.org/pdb/home/home.do (accessed Dec 7, 2016), PDB ID 1T0T, released Aug 4, 2004.

(24) Gonzalez, A.; Tsai, Y. http://smb.slac.stanford.edu/facilities/software/xds/#autoxds_script (accessed May 1, 2016).

(25) McCoy, A. J.; Grosse-Kunstleve, R. W.; Adams, P. D.; Winn, M. D.; Storoni, L. C.; Read, R. J. *J. Appl. Crystallogr.* **2007**, *40*, 658−674.

(26) Winn, M. D.; Ballard, C. C.; Cowtan, K. D.; Dodson, E. J.; Emsley, P.; Evans, P. R.; Keegan, R. M.; Krissinel, E. B.; Leslie, A. G.; McCoy, A.; McNicholas, S. J.; Murshudov, G. N.; Pannu, N. S.; Potterton, E. A.; Powell, H. R.; Read, R. J.; Vagin, A.; Wilson, K. S. *Acta Crystallogr., Sect. D: Biol. Crystallogr.* **2011**, *67*, 235−42.

(27) Adams, P. D.; Afonine, P. V.; Bunkóczi, G.; Chen, V. B.; Davis, I. W.; Echols, N.; Headd, J. J.; Hung, L. W.; Kapral, G. J.; Grosse-Kunstleve, R. W.; McCoy, A. J.; Moriarty, N. W.; Oeffner, R.; Read, R. J.; Richardson, D. C.; Richardson, J. S.; Terwilliger, T. C.; Zwart, P. H. *Acta Crystallogr., Sect. D: Biol. Crystallogr.* **2010**, *66*, 213−21.

(28) Mayfield, J. A.; Hammer, N. D.; Kurker, R. C.; Chen, T. K.; Ojha, S.; Skaar, E. P.; DuBois, J. L. *J. Biol. Chem.* **2013**, *288*, 23488−504.

(29) Celis, A.; DuBois, J. *Arch. Biochem. Biophys.* **2015**, *574*, 3−17.

(30) Goblirsch, B.; Kurker, R. C.; Streit, B. R.; Wilmot, C. M.; DuBois, J. L. *J. Mol. Biol.* **2011**, *408*, 379−398.

(31) Hofbauer, S.; Dalla Sega, M.; Scheiblbrandner, S.; Jandova, Z.; Schaffner, I.; Mlynek, G.; Djinovic-Carugo, K.; Battistuzzi, G.; Furtmüller, P. G.; Oostenbrink, C.; Obinger, C. *Biochemistry* **2016**, *55*, 5398−5412.

(32) Hofbauer, S.; Howes, B. D.; Flego, N.; Pirker, K. F.; Schaffner, I.; Mlynek, G.; Djinović-Carugo, K.; Furtmüller, P. G.; Smulevich, G.; Obinger, C. *Biosci. Rep.* **2016**, *36*, e00312.

(33) Choudhury, K.; Sundaramoorthy, M.; Hickman, A.; Yonetani, T.; Woehl, E.; Dunn, M. F.; Poulos, T. L. *J. Biol. Chem.* **1994**, *269*, 20239−20249.

(34) Poulos, T. L.; Fenna, R. E., Peroxidases—Structure, Function, and Engineering. In *Metal Ions In Biological Systems, Vol 30*; Wiley VCH; New York, 1994.

(35) Blanc, B.; Mayfield, J. A.; McDonald, C. A.; Lukat-Rodgers, G. S.; Rodgers, K. R.; DuBois, J. L. *Biochemistry* **2012**, *51*, 1895−1910.

(36) Singh, R.; Grigg, J. C.; Armstrong, Z.; Murphy, M. E. P.; Eltis, L. D. *J. Biol. Chem.* **2012**, *287*, 10623−10630.

(37) Erman, J. E.; Vitello, L. B.; Miller, M. A.; Kraut, J. *J. Am. Chem. Soc.* **1992**, *114*, 6592−6593.

(38) Layer, G.; Pierik, A. J.; Trost, M.; Rigby, S. E.; Leech, H. K.; Grage, K.; Breckau, D.; Astner, I.; Jaensch, L.; Heathcote, P.; Warren, M. J.; Heinz, D. W.; Jahn, D. *J. Biol. Chem.* **2006**, *281*, 15727−34.

(39) Draganova, E. B.; Adrian, S. A.; Lukat-Rodgers, G. S.; Keutcha, C. S.; Schmitt, M. P.; Rodgers, K. R.; Dixon, D. W. *JBIC, J. Biol. Inorg. Chem.* **2016**, *21*, 875−86.

(40) Spiro, T. G.; Soldatova, A. V.; Balakrishnan, G. *Coord. Chem. Rev.* **2013**, *257*, 511−527.

(41) Lukat-Rodgers, G. S.; Rodgers, K. R.; Caillet-Saguy, C.; Izadi-Pruneyre, N.; Lecroisey, A. *Biochemistry* **2008**, *47*, 2087−2098.

(42) Spiro, T. G.; Wasbotten, I. H. *J. Inorg. Biochem.* **2005**, *99*, 34−44.

(43) Blanc, B.; Mayfield, J. A.; McDonald, C. A.; Lukat-Rodgers, G. S.; Rodgers, K. R.; DuBois, J. L. *Biochemistry* **2012**, *51*, 1895−1910.

(44) Hofbauer, S.; Howes, B. D.; Flego, N.; Pirker, K. F.; Schaffner, I.; Mlynek, G.; Djinovic-Carugo, K.; Furtmueller, P. G.; Smulevich, G.; Obinger, C. *Biosci. Rep.* **2016**, *36*, e00312.

(45) Goblirsch, B. R.; Streit, B. R.; DuBois, J. L.; Wilmot, C. M. *JBIC, J. Biol. Inorg. Chem.* **2010**, *15*, 879−888.

(46) Streit, B. R.; Blanc, B.; Lukat-Rodgers, G. S.; Rodgers, K. R.; DuBois, J. L. *J. Am. Chem. Soc.* **2010**, *132*, 5711−5724.

(47) Hofbauer, S.; Gruber, C.; Pirker, K.; Schaffner, I.; Furtmuller, P.; Obinger, C.; Hagmuller, A.; Gysel, K.; Mlynek, G.; Kostan, J.; Djinovic-Carugo, K.; Bellei, M.; Battistuzzi, G.; Daims, H. *Biochemistry* **2014**, *19*, 53−77.

(48) Grant, J. L.; Hsieh, C. H.; Makris, T. M. *J. Am. Chem. Soc.* **2015**, *137*, 4940−4943.

(49) Zheng, Y. M.; Baer, B. R.; Kneller, M. B.; Henne, K. R.; Kunze, K. L. *Biochemistry* **2003**, *42*, 4601−4606.

(50) Colas, C.; Ortiz de Montellano, P. R. *Chem. Rev.* **2003**, *103*, 2305−2332.

(51) Brown, K. R.; Brown, B. M.; Hoagland, E.; Mayne, C. L.; Hegg, E. L. *Biochemistry* **2004**, *43*, 8616−8624.

(52) Stubbe, J.; Nocera, D. G.; Yee, C. S.; Chang, M. C. Y. *Chem. Rev.* **2003**, *103*, 2167−2201.

(53) Okamura, M. Y.; Paddock, M. L.; Graige, M. S.; Feher, G. *Biochim. Biophys. Acta, Bioenerg.* **2000**, *1458*, 148−163.

(54) Whittaker, J. W. *Chem. Rev.* **2003**, *103*, 2347−2363.

(55) Tsai, A. L.; Kulmacz, R. J.; Palmer, G. *J. Biol. Chem.* **1995**, *270*, 10503−10508.

(56) Warren, J. J.; Tronic, T. A.; Mayer, J. M. *Chem. Rev.* **2010**, *110*, 6961−7001.

(57) Hofbauer, S.; Mlynek, G.; Millazo, L.; Pühringer, D.; Maresch, D.; Schaffner, I.; Furtmüller, P. G.; Smulevich, G.; Djinović-Carugo, K.; Obinger, C. Hydrogen Peroxide Mediated Conversion of Coproheme to Heme *b* by HemQ. Lessons from the First Crystal Structure and Kinetic Studies. FEBS J. [Online early access]. doi: 10.1111/febs.13930. Published Online: Nov 14, 2016. http://onlinelibrary.wiley.com/wol1/doi/10.1111/febs.13930/abstract (accessed Oct 30, 2016).